doi.org/10.15392/2319-0612.2025.2633
Braz. J. Radiat. Sci., Rio de Janeiro
2025, 13(1) | 01-40 | e2633
Editor: Prof. Dr. Bernardo Maranhão Dantas
Editor: Prof. Dr. Alfredo Lopes Ferreira Filho
Submitted: 2024-08-26
Accepted: 2025-01-07

A neoteric technique to validate radon-222 transport modelling from a gold mine tailings dam

Komati[a*], F. S.; Ntwaeaborwa[b], O. M; Strydom[c], R.

[a] Department of Mathematical and Physical Sciences, Central University of Technology, Private Bag X20539, Bloemfontein, 9300, South Africa
[b] Faculty of Natural Sciences, Sol Plaatje University, 10 Jan Smuts Blvd, Civic Centre, Kimberely, 8300, South Africa
[c] Parc Scientific, P O Box 1045, Cresta, 2118, South Africa

*Correspondence: fkomati@cut.ac.za / komatifrank@gmail.com (F.S. Komati)

Abstract: The Gaussian Industrial Source Complex Short Term 3 (ISCST3) model as applied to radon-222 emitted from tailings dams has not been properly validated for radon-222 dispersion modelling. In an attempt to validate the model, the concentrations of radon-222 and its progenies/daughters were measured at various points around a tailings dam. To verify that the measured radon-222 is from the tailings dam, a technique combining both gas and daughters ages with source apportionment method was developed. Model was validated by isolating radon-222 from different sources using the "age" of the gas approach and applying back trajectory calculations to identify the origin of the radon gas measured at points downwind. As predicted by the model, the origin of the radon emission was traced back to the tailings. The model was further validated by comparing measured data to model outputs and applying standard model validation statistics to validate and quantify the agreement between predicted and measured data. Model validation from statistical analysis showed a constant trend with minimum variability in the Index of Agreement (IOA), Normalized Mean Square Error (NMSE), and Fraction of Predictions method within a factor of two (FAC2) values. The analyses were based on the model prediction results over five days of measurements covering both morning and afternoon. There was an under prediction in the Fractional Bias (FB) and Geometric Mean bias (MG) in the afternoon of day 1. In addition, the model performed poorly in the afternoon of day 3.

Keywords: atmospheric dispersion, radon progeny, model validation, background radon, back trajectories

doi.org/10.15392/2319-0612.2025.2633
Braz. J. Radiat. Sci., Rio de Janeiro
2025, 13(1) | 01-40 | e2633
Editor: Prof. Dr. Bernardo Maranhão Dantas
Editor: Prof. Dr. Alfredo Lopes Ferreira Filho
Submitted: 2024-08-26
Accepted: 2025-01-07

Uma técnica neotérica para validar a modelagem de transporte de radônio-222 a partir de uma barragem de rejeitos de uma mina de ouro

Resumo: O modelo Gaussian Industrial Source Complex Short Term 3 (ISCST3), aplicado ao radônio-222 emitido de barragens de rejeitos, não foi devidamente validado para a modelagem de dispersão de radônio-222. Com o objetivo de validar o modelo, as concentrações de radônio-222 e seus produtos de decaimento/filhas foram medidas em vários pontos ao redor de uma barragem de rejeitos. Para verificar se o radônio-222 medido provinha da barragem, foi desenvolvida uma técnica que combina as idades do gás e de suas filhas com o método de atribuição de fontes. O modelo foi validado isolando o radônio-222 de diferentes fontes, utilizando a abordagem da "idade" do gás e aplicando cálculos de trajetórias inversas para identificar a origem do radônio medido em pontos a favor do vento. Conforme previsto pelo modelo, a origem da emissão de radônio foi rastreada até a barragem de rejeitos. O modelo foi ainda validado comparando-se os dados medidos com os resultados do modelo e aplicando estatísticas padrão de validação de modelos para verificar e quantificar a concordância entre os dados previstos e os medidos. A validação do modelo, com base na análise estatística, mostrou uma tendência constante com mínima variabilidade nos valores do Índice de Concordância (IOA), do Erro Quadrático Médio Normalizado (NMSE) e do método da Fração de Previsões dentro de um fator de dois (FAC2). As análises foram realizadas com base nos resultados das previsões do modelo ao longo de cinco dias de medições, abrangendo tanto o período da manhã quanto o da tarde. Houve uma subestimação no Viés Fracionado (FB) e no Viés Médio Geométrico (MG) no período da tarde do primeiro dia. Além disso, o modelo apresentou baixo desempenho no período da tarde do terceiro dia.

Palavras-chave: dispersão atmosférica, progenitores do radônio, validação do modelo, radônio de fundo, trajetórias retroativas.

1. INTRODUCTION

Anthropogenic activities like gold, uranium and coal mining activities, oil and gas exploration, phosphate fertilizer production and Naturally Occurring Radioactive Materials (NORM) repositories such as phosphogypsum stacks, building materials and waste dumps from gold activities have eventually found their way into various environmental sectors [1–3]. One of the main issues of environmental pollution from gold mining in South Africa is the widespread environmental distribution of uranium and its decay progenies, particularly radioactive radon (^{222}Rn) gas (hereafter referred to as "radon") [4]. As reported in [5], South Africa's underground gold reserves contain low-grade uranium (^{238}U) and, over the years, millions of tons of uranium-bearing rocks and unwanted radioactive materials have been brought to the surface by gold mining activities [6]. After the milling and gold extraction processes, uranium and subsequently radium (^{226}Ra) bearing tailings are disposed of as waste on large tailings dams [7]. Consequently, these tailings may contribute to environmental radiation and become important sources of radon gas [8]. In regions near gold mines, this could lead to a marginal increase in public exposure above acceptable levels [9, 10].

Radon, an inert, colourless and odourless gas with a half-life of 3.8 days, originate from the alpha decay of ^{226}Ra in the tailings material. It diffuses to the surface of the dam, and is released and dispersed into the surroundings in large quantities. Radon decays by emitting an alpha particle to produce several short-lived progenies. The short-lived progenies of interest in this study and their half-lives are ^{218}Po (RaA; 3.05 min), ^{214}Pb (RaB; 26.8 min), ^{214}Bi (RaC; 19.7 min). As a gas, radon can be inhaled; once within lungs (and along with its progenies) it may lead to cancer [11–13].

The introduction and dispersion of radon from the tailings dam into the atmosphere is a function of bulk air movements and transport, convective diffusion, release

concentration and height, atmospheric stability, vertical temperature gradient, wind strength, speed and direction, air turbulence, etc. [14, 15]. As a gas, radon is expected to mix up and concentrate in air (outdoor atmosphere) while its concentration will decrease with distance from the tailings [16]. The short-lived progenies on the other hand, attach to airborne particles e.g. smoke or grow in size through water vapour nucleation and condensation to form attached and unattached fractions. The later radioactive daughter nuclides grow in overtime according to their half-lives and assume transport properties of the aerosol. Through vertical and horizontal transport of aerosol particles in the atmospheric boundary layer, these alpha particle emitters can then be dispersed away from the radon source [17]. Hence, monitoring and assessing radon and progeny concentrations at some distances from such facilities, especially when they are near residential areas or sensitive receptors, are necessary for regulatory health risk evaluation [16].

Measurements of atmospheric radon progeny activity concentrations are also important for determining the "age" of the gas after some release time and for evaluating effective radiation dose. Their concentrations and that of radon in air vary from time to time due to changes in meteorological conditions such as temperature, wind speed, rainfall, etc. Subsequently, radon and its progenies in the outdoor atmosphere are not in secular equilibrium. The disequilibrium between radon and its three short-lived progenies can be quantified by the equilibrium factor, often referred to as F factor. The equilibrium factor can be interpreted as a good indicator of the "age" of a Rn-222/progeny mixture. In the context of this paper, "old" radon refers to radon mixed with accumulated radon daughters. This radon is more harzadous for lung cancer when inhaled due to the presence of the short-lived alpha decaying radon daughters. Othe other hand, "fresh" radon, originating from radium-226 decay, has not yet accumulated significant levels of radon daughters, making it less immediately hazardous compared to "old" radon."

High radon concentration values compared to progenies, and hence low equilibrium factor, indicate that radon at that receptor point is still "fresh". This low equilibrium factor occurs when there is high disequilibrium between radon and its progeny concentrations in the atmosphere. Under these conditions, radon is expected to be of "local" origin, instead of radon transported from other distant sources. Inasmuch as time and distance augment from source, radon gets 'older' and decays into respective daughters, thus increasing the equilibrium factor.

Information on atmospheric radon origin constitutes an important step in assessing radiological environmental impact as it helps selection and implementation of appropriate mitigation strategies in cases of high radon levels. Currently, monitoring techniques directly measuring atmospheric radon concentrations nearby tailings dams only establish its presence in the surroundings. These techniques, however, are unable to distinguish between background radon and radon from tailings, nor can they quantify the relative contributions of multiple sources to atmospheric radon content. For this reason, air dispersion modelling is used as an alternative to or as support for monitoring, to ascertain the location of radon source (origin) and to assess radon impact related to tailings dams. Atmospheric dispersion models employ sophisticated mathematical codes to predict the movement and distribution of pollutants within the atmosphere. These models incorporate key meteorological and environmental conditions, particularly those dominating the atmospheric boundary layer. By integrating critical factors such as wind speed, atmospheric turbulence, and thermodynamic effects, these models enable predictions of the convective diffusion rates of pollutants.

When using modeling for prediction exercises, it is crucial to evaluate and validate both the model's performance and the accuracy of its predictions. Rigorous evaluation helps identify potential biases, overfitting, or underfitting, while validation confirms that the model performs consistently across various datasets or scenarios.

Uncertainty in dispersion model predictions arises from a variety of factors, including the idealisations inherent to any mathematical model, the appropriateness of the model chosen for a particular application, and the values attributed to the various model parameters. Besides, model input data are based on assumptions and calculations using empirical formulas and, as such, the accuracy of these calculations and presumptions will influence the accuracy of model results. Therefore, model validation becomes a critical component of modeling research that determines whether a model generates accurate and dependable results [18]. Hence, validating dispersion models against numerical data from real-world dispersion events is one of the important steps in model development [19].

In this study, the steady-state Gaussian plume Industrial Source Complex Short Term 3 (ISCST3) commercial atmospheric dispersion software developed by BREEZE AERMOD GIS Pro (Version 4.0., Trinity Consultants Inc., Dallas, TX, USA, 2002) was used to calculate and predict radon concentrations from a tailings dam at specified downwind receptor points. The output is a 2-dimensional field of pollutant concentration in the atmosphere expressed in terms of activity concentration in air [Bq/m^3]. As an EPA (U.S. Environmental Protection Agency) model designed to reinforce regulatory modelling programs [20], ISCST3 was developed to simulate atmospheric pollutants from point or area sources using emission rates and meteorological data as model inputs.

For this study, choice and preference of the ISCST3 over other Gaussian models (AERMOD, ADMS, etc.) was due to its relative operation ease, ruggedness and reproducible prognoses [21]. The model was also found to outperform the recently EPA approved AERMOD under stable climatic conditions [22] and simple flat terrains [23] as it was the case in this study. Furthermore, the main advantage of choosing the ISCST3 over AERMOD is that it uses true measured local weather data, thus prospectively leading to more accurate results on the small-scale of this project whereas AERMOD uses data from mesoscale meteorological models.

Notably, the HYSPLIT model is another widely used tool in atmospheric sciences for analyzing air mass trajectories (both forward and backward) and dispersion [15, 17, 24, 25]. It combines Lagrangian and Eulerian methods: the Lagrangian approach tracks air parcels for advection and diffusion, while the Eulerian framework calculates pollutant concentrations using a fixed 3-D grid [26]. Yet, the model is subject to inaccuracies which include trajectory location errors estimated at 15-30% of the distance travelled [27, 28]. These errors arise from physical inaccuracies in representing atmospheric conditions like wind components and numerical challenges like integration and truncation errors [29]. Similar to other models, the model's accuracy also depends on the quality and availability of input data [30]. Despite its practicality, HYSPLIT is not recommended by U.S. EPA for regulatory purposes, instead a steady-state Gaussian plume dispersion model, AERMOD (and previously ISCST3) is the preferred model for estimating point source impacts.

Throughout the course of time, the ISCST3 dispersion model has been comprehensively evaluated and validated for point and area sources on atmospheric dispersion of odours, NOx, SO_2, CO_2, bio aerosol emissions, agricultural sources, ammonia (NH_3) and particulate matter (PM_{10}) [31–34]. [35] and [36] discussed and reported various ISCST3 performance evaluation and validating studies as well as their results from point, area and volume source field data. Results showed a good agreement between predicted concentrations and observed counterparts, particularly for point sources. However, no data is available for ISC dispersion model evaluation and validation for outdoor radon from tailings dams.

The primary aim of this study was to identify and apportion the sources of radon emissions, and to validate the model by measuring radon concentrations at a specific receptor point. This was achieved using a dispersion model and the 'age' of the gas approach to estimate the radon levels originating from the tailings dam. While an equilibrium factor approach was also investigated by [37], this study proposes a novel, more direct and accurate

method. This strategy focuses on measuring the concentration of radon-222 and its progeny at various distances from the dam under different environmental conditions. By analyzing these measurements, the activity concentration ratios of radon to its individual progeny will be calculated. These ratios serve to estimate the "age" of the radon gas, providing insights into its origin.

In addition, the model's performance was evaluated using standard validation statistical descriptors developed by EPA and the American Meteorological Society. These descriptors, pointed out by [30], [31], and [32], help correlate model predictions with field measurements.

This study was initially carried out as a component of the author's thesis at Central University of Technology, Bloemfontein [41]. This manuscript disseminates and expands upon techniques, findings, and analysis that were developed and produced in aforesaid thesis.

2. MATERIALS AND METHODS

2.1. Study area

The long half-life of radon (3.8 days) enables its transport over significant distances through advective motion in air currents. Consequently, radon from distant sources can be detected at monitoring sites. Atmospheric radon levels exhibit variation based on wind velocity, which influences both locally emitted radon and radon transported from other regions. To minimize the influence of external sources, such as nearby tailings dams or other anthropogenic radon emitters, a remote tailings dam located on flat terrain was deemed ideal and appropriate for this study. As such, an “isolated” dry and dormant tailings dam (Figure 1) containing gold mine tailings from an old, closed mine shaft was chosen for the study.

The 30 m high dam with ground-level base area of 1.08 x 10^8 m^2 is situated in the Lejweleputswa District Municipality, Free State Province, (South Africa) between

Odendaalsrus (-27°51'59.99" S 26°40'59.99" E) and Allanridge (27°45'15.52"S, 26°38'37.75"E) towns. The tailings dam is surrounded by a settlement to the north, by a road (namely, R30) and a plantation farm to the west, a small lake, and a hostel inhabited by about two hundred people to the southeast of the tailings. The nearest tailings dam, which is still "active" with wet sludge from the adjacent operational gold mine, is about 5 km northwest of the tailings dam. Other tailings dams are located at 8.6 km and 16 km respectively on the south and south-east side of the tailings. There are no other tailings dams or man-made sources in the north, north-east and east of the dam, the wind directions along which measurements were undertaken. There are no tailings dams or artificial sources located to the north, northeast, or east of the dam, which are the directions where measurements were taken.

Figure 1: Aerial view of tailings dam (Google Earth®).

Local meteorological 5-days data for the study location was obtained from the South African Weather Service (SAWS) from August 19 to August 27, 2017. Data was specifically collected on the following days: Day 1 (19/08/2017), day 2 (20/08/2017, day 3 (21/08/2017), day 4 (26/08/2017) and day 5 (27/08/2017).The high-resolution 5-minutes weather measurements were obtained using the automatic weather station (AWS) technology

deployed in Welkom, about 2 km from the tailings dam. The anemometer was placed in an open and level terrain, with measurements taken at 10 m above ground level in accordance with the World Meteorological Organisation (WMO) standards. Due to safety and security concerns as well as high costs of portable weather station, it was not advisable and feasible to place a weather station at the data collection. During the winter months of June through August, the area was characterised by a predominance of average winds from the north, north-east, and north-west. For days 1 (100%) and 4 (100%), the primary directions were north-east; for days 2 (50%), north; and for days 3 (100%) and 5 (90%), north-west. There was no rain or precipitation during the data collection period, and the average daily minimum and maximum temperatures ranged from 9°C to 20°C.

2.2. Radon-22 and its daughter measurements

Grab sampling using a single filter method was used to measure radon daughter concentrations from the outdoor environment around the tailings dam. Sample collection and counting were conducted in the field at each sampling point. Radon daughters were collected by drawing outdoor air at a height of about 1.5 m from the ground level and deposited onto a filter for 10 minutes, followed by gross alpha counting. The deposited daughter particles were detected using Eberline Model SPA-1A ZnS(Ag) scintillation detector and counting was performed with Eberline Smart Portable (ESP-2) counter. The counter was operated in the Integrated Scaler mode to obtain total gross counts in accordance with Busigin and Phillips [42] counting method. ESP-2 is factory calibrated for immediate use and can store up to three sets of detector calibration parameters. To ensure that the correct calibration parameters for Eberline Model SPA-1A scintillation detector match the parameters listed on the calibration certificate, the supplied calibration parameters were re-entered into ESP-2 prior to operation.

After calibration, an Americium-241 reference source (verified to produce approximately 1410 counts per five minutes) was used to test ESP-2's response to a check source to assure

acceptable operation. The measured five-minute counts were 1250, thus producing a ±11% deviation which was deemed to be an acceptable systematic error of the counter. In addition, precision of ESP-2 alpha counter's performance and results reproducibility were evaluated using chi-square ($\chi 2$) test as stipulated in IAEA technical document [43]. According to this technical document, chi-square value is acceptable if it falls between 3.33 and 16.92 for a set of 10 measurements. Chi-square value for this counter was found to be 8.10, well within the recommended range of 3.33 to 16.92 for a well-performing counter [44].

Individual radon daughter concentrations (Bq/m^3) were calculated using the set of three Busigin and Phillips equations corresponding to the counting intervals of 2 – 5, 7 – 15, and 25 – 30 minutes which were modified, optimised and corrected by [45]. The equations used are:

$$C_{218_{Po}} = \frac{1}{FE}[6.2241C_1 - 4.231C_2 + 3.441C_3 - 2.0247R_b] \quad (1)$$

$$C_{214_{Pb}} = \frac{1}{FE}[-0.03019C_1 - 0.91247C_2 + 2.6563C_3 - 5.8913R_b] \quad (2)$$

$$C_{214_{Bi}} = \frac{1}{FE}[-0.80797C_1 + 1.68C_2 - 1.7755C_3 - 2.1388R_b] \quad (3)$$

where

F flow rate in L/min;

E alpha counting efficiency (60%) in cpm/dpm;

R_b background count rate in cpm;

C_1 gross count in interval 2-5 minutes after sampling (3-minute count);

C_2 gross count in interval 7-15 minutes after sampling (8-minute count); and

C_3 gross count in interval 25-30 minutes after sampling (5-minute count).

A pulse chamber AlphaGUARD PQ2000 PRO model active radon monitor with a detection efficiency of 5 cpm at 100 Bq/m^3 (3 pCi/L) and an instrument calibration error

(type B) of 3% (plus uncertainty of the primary standard) were used to measure radon concentrations at identified receptor points. Placed at a height of about 1.5 m, the monitor was operated in flow mode with 10-minute cycles, which corresponds to a 10-minute sampling period for the radon daughter measurements. Therefore, the total radon measurement time at on measuring point was 10 minutes. Seven sets of downwind data were collected, three in the morning and four in the afternoon as shown in Figure 2.

Uncertainty approximations from all possible uncertainty sources such as background counting, sampling and calibration were estimated using the Guide to the Expression of Uncertainty in Measurement (GUM) [46]. Uncertainties propagation law was applied to combine individual uncertainty components related to systematic and statistical errors. Poisson distribution was utilised to compute the counting uncertainties (Type A) for AlphaGUARD and ESP-2 alpha counter. Uncertainty in the number of counts was expressed at 1-sigma range and correction factor of $k = 1$.

As shown in Figure 2, airborne radon and progeny concentrations were each measured simultaneously at different receptor points downwind of a tailings dam by following the wind direction at time intervals of approximately 1 hour between successive measurements from tailings base. Mean wind speed and direction were considered to be constant over the entire sampling period. The measuring distances varied between 100 m and 200 m depending on accessibility and suitability. Similarly, upwind measurements shown in Figure 3 were also taken and used as background.

Figure 2: Downwind sampling points for (a) day 1 morning, (b) day 1 afternoon, (c) day 2 afternoon, (d) day 3 morning, (e) day 3 afternoon, (f) day 4 afternoon and (g) day 5 morning.

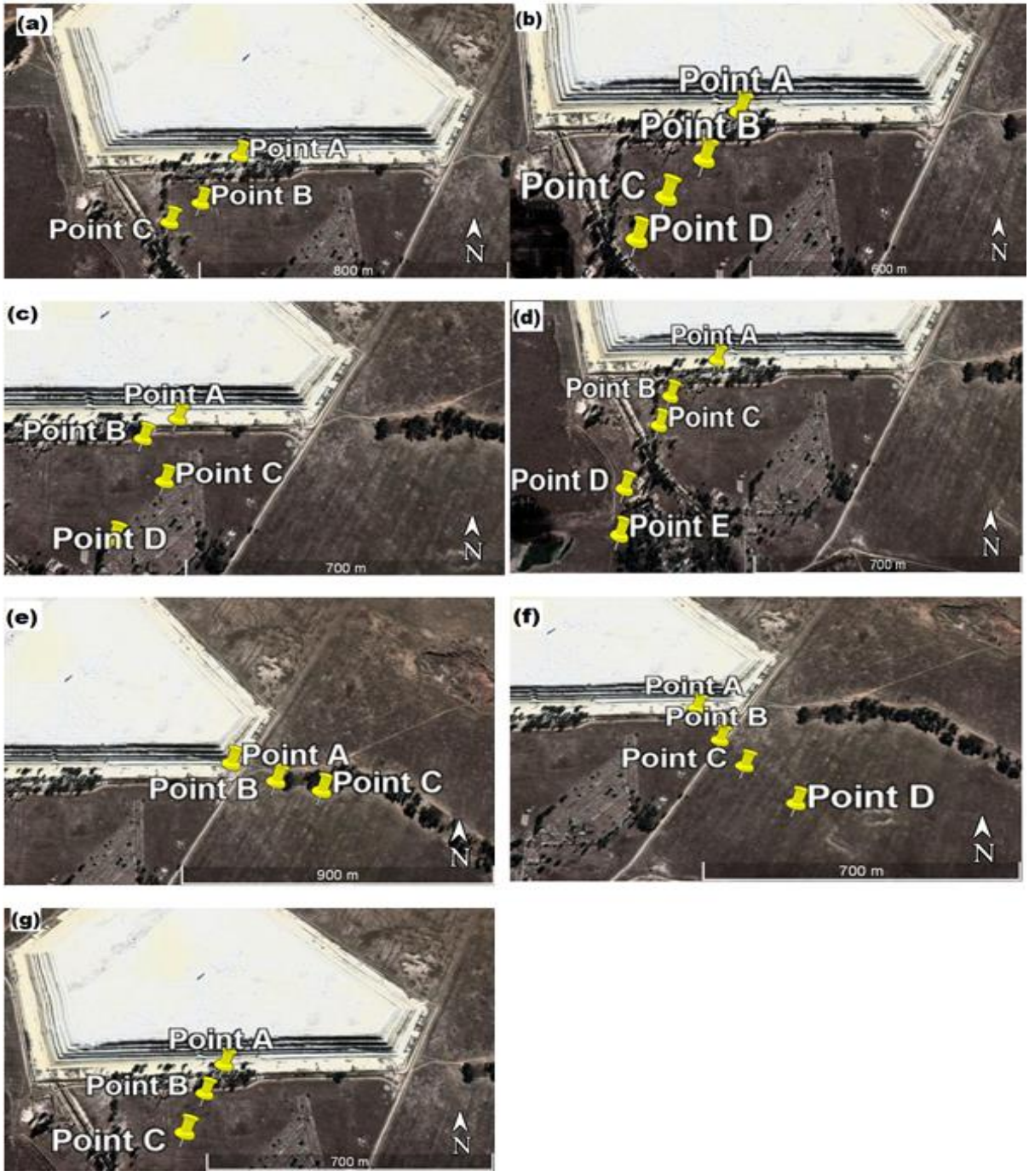

Figure 3: Upwind sampling points

Modelling protocol and procedures, including input data described in this study and summarised below, are fully outlined and explained by [47]. This study models the tailings dam as 2-D source with a priori known emitting surface area of the dam. Modelled concentrations were calculated for 1 hour averaging periods. ISCST3 model was run in concentration mode using USEPA regulatory default options, 1-h concentration option, non-regulatory rural dispersion coefficients and the receptor height of 1.5 m.

The study applied the following main modelling inputs from the source/emission options: number of sources (multiple sources from all sides of the tailings); output contribution (combined pollutant concentrations from all sides); source type (area); height of the tailings dam (30 m); height of the sources (varied from 0 at ground flat surface to 30 m at dam top); and area shape (polygon). The main output was ^{222}Radon concentrations in μ Bq m^{-3}, which was converted to Bq m^{-3}. A steady-state area-weighted emission rate of 0.102 Bq m^{-2} s^{-1} experimentally measured by [48] was used for all area sources.

Five-minute weather data from 19–27 August 2017, for the Welkom – Odendaalsrus region obtained from the South African Weather Service (SAWS) at an anemometer height of 10 m was processed and averaged to produce hourly data. to produce hourly data. Also, five meteorological data files, one for each day of measurements, were formatted as FORTRAN executable ASCII files. Aforesaid data pre-processing aimed at suitability for ISCST3 model. ISCST3 modeling only takes into consideration airborne radon concentrations exhalated from the tailings dam.

To determine the total radon concentration at a receptor site, the modelled radon concentrations were combined with the background radon concentration. The background concentration was measured "upwind" of the tailings dam along the same line and wind direction as the modeled "downwind"concentration. This approach ensures that background radon levels are appropriately accounted for when assessing total radon concentration at receptor site.Wind variation of $\pm 10^0$ was allowed because there is no significant change in concentration within this degree range [49].

2.3. Model validation - Statistical analysis

Addresses shortly ahead, statistical model performance used the following variables:

C_O: Observed (measured) concentration;

C_P: Modeled concentration; and

Overbar: average over the whole dataset.

The statistical methods used were:

(a) Index of agreement (IOA) (*d*)

$$d = 1 - \frac{\sum_{i=1}^{n}(C_P - C_O)^2}{\sum_{i=1}^{n}(|C_P - \overline{C_O}| + |C_O - \overline{C_O})|^2} \quad (4)$$

(b) Fractional Bias (FB)

$$FB = 2x\left(\frac{\overline{C_O} - \overline{C_P}}{\overline{C_O} + \overline{C_P}}\right) \quad (5)$$

(c) Geometric Mean Bias (MG)

$$MG = exp\left(\overline{lnC_O} - \overline{lnC_P}\right) \quad (6)$$

(d) Normalised Mean Square Error (NMSE)

$$NMSE = \frac{\overline{(C_O - C_P)^2}}{\overline{C_O} \text{ x } \overline{C_P}} \quad (7)$$

(e) Fraction of predictions within a factor of two (FAC2)

$$FAC2 = fraction\ of\ data\ that\ satisfy\ 0.5 \leq \frac{C_P}{C_O} \leq 2.0 \quad (8)$$

There is no universal method applicable to all modelling conditions. Multiple statistical performance parameters are recommended because each has either advantages or disadvantages in view of the variable distribution [18]. Based on guidelines proposed by [50], this study used the following criteria to assess reliability and performance of ISCST3 model:

$$0.4 \leq d \leq 1.0$$

$$NMSE < 0.5$$

$$-0.5 < FB < +0.5$$

$$FAC2 > 0.8$$

$$0.75 < MG < +1.25$$

In terms of performance assessment, calculations from ISCST3 model are classified as 'under-prediction', 'exact prediction' and 'over-prediction'.

2.4. Model validation - Source apportionment using "gas age" approach

Radon and its daughter concentrations were hourly measured at different receptor points by following the wind direction ("follow the wind" approach). At each receptor, radon daughter to radon ratios, i.e. RaA/Rn and RaB/Rn, were calculated from measured radon, RaA, and RaB concentrations. From radon daughter measurements, RaA and RaB concentrations were dominant while RaC counterpart was mostly undetectable. It was therefore deemed prudent prudent to limit radon daughter to radon activity ratios to concentrations from radon, RaA and RaB .

Calculated ratios and fractional activity graph of short-lived radon daughters growing towards the radon level as a function of time were used to estimate radon transit time (= time necessary for measured daughter level to grow in) from the tailings to the receptor. The graph was filled by standardizing the pure radon concentration to an activity of 1 Bq/m^3 at time $t = 0$. Radon decay and radon daughter's ingrowth (RaA and RaB) over time were calculated using Bateman's equations. The normalised graph is presented in Figure 4.

Figure 4: Normalised in-growth of radon daughters' activities of an atmosphere initially containing pure ^{222}Rn

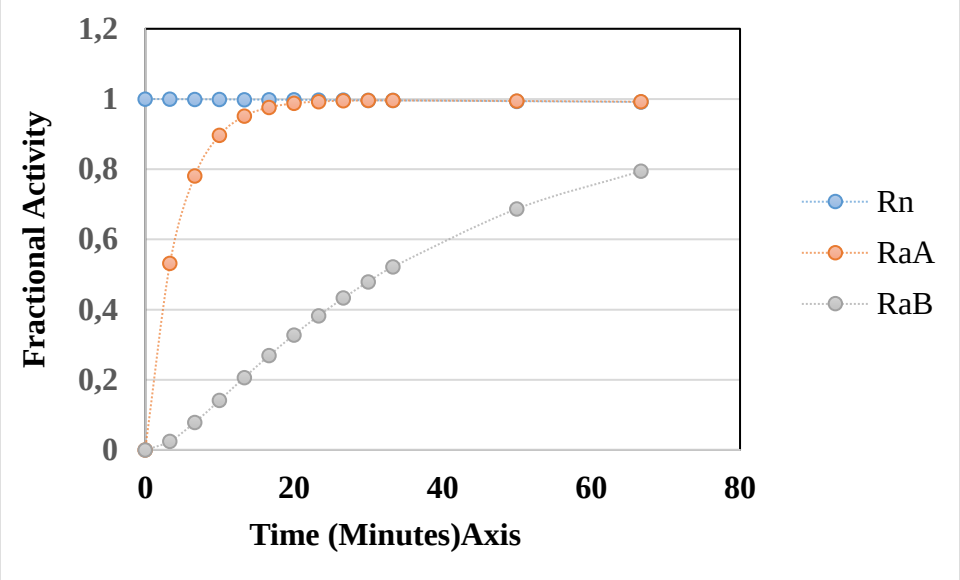

Using the measured activity ratios for both RaA and RaB, radon travel time from the source (tailings) to each receptor, or the "age" of the gas from the dam, was extrapolated from the graph in Figure 4. The estimated times and the corresponding mean wind velocities from weather data were then used to calculate the reverse distances from source (tailings) to each receptor, i.e. 'gas age' from the dam.

This method of determining the source-receptor relationship and tracing back the origin of the modeled and measured radon concentrations at the receptor represents a kinematic back trajectory calculation of the air mass moving from the tailings to the receptor and was applied to estimate the distance from source to receptor. Similar work was reported by [27]. Accordingly, given the velocity (v, m/s) of radon from the tailings (wind velocity) and the transit step time ($\measuredangle t$) obtained from the diagram in Figure 4, the backward distance (i.e. starting position) was calculated from the equation:

$$x(t) = \Delta t \cdot v(t_0) \tag{9}$$

The application of equation (9) was based on the horizontal straight-line distance traveled from the source to the receptor. Atmospheric turbulent mixing, meteorological parameters and vertical transport were not considered in the application of equation (9). Using a single back calculation for short-distance radon transport introduces the potential for uncertainties and errors. However, for short time scales, as in this study, equation (9) can be considered to be a sufficient screening calculation [27].

When applying this progeny-based indirect radon detection approach, it was further assumed that weather conditions remained calm with no precipitation during sampling periods. Each measuring point was treated independently, with the time difference between consecutive "follow the wind" measurements being approximately one hour. Calculated source points and distances from the receptor were plotted into *Google Earth*® to locate their positions relative to the tailings dam and numerical results were compared to their measured counterparts.

3. RESULTS AND DISCUSSIONS

3.1. Measured vs modelled radon concentrations

Calculated and measured radon concentrations at all receptors are graphically presented in Figure 5 (a – g).

Figure 5: Graphical presentation of measured and modelled concentrations.

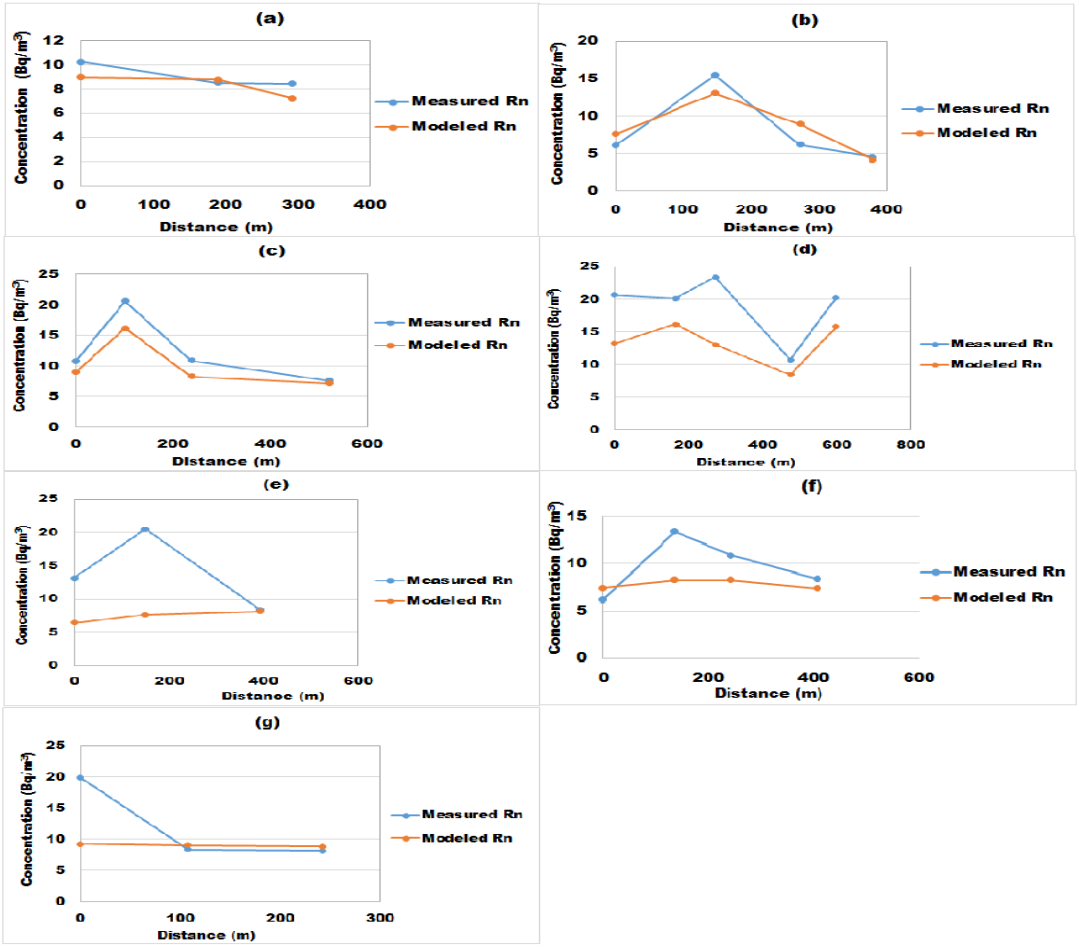

3.2. Model validation: Statistical analysis

Table 1 presents the results from the statistical parameters used to quantitatively assess the performance of the ISCST3 model. These values were calculated using equations (4) – (8).

Table 1 : Statistical analysis and model performance assessment

Day	Measured mean (Bq/m³)	Modelled mean (Bq/m³)	IOA (0.4 - 1.0)	FB (-0.5 - +0.5)	MG (0.75 - +1.25)	NMSE (< 0.5)	FAC2 (> 0.8)
Day 1 Morning	9.063	8.339	0.632	0.083	1.087	0.013	1.087
Day 1 Afternoon	8.113	8.527	0.926	-0.05	0.951	0.059	0.951
Day 2 Afternoon	12.495	10.209	0.902	0.201	1.224	0.058	1.224
Day 3 Morning	19.016	13.353	0.637	0.350	1.424	0.158	1.424
Day 3 Afternoon	14.003	7.422	0.431	0.614	1.887	0.670	1.887
Day 4 Afternoon	9.708	7.900	0.551	0.205	1.229	0.113	1.229
Day 5 Morning	12.107	9.042	0.466	0.290	1.339	0.346	1.339

The index of agreement (IOA) *d* shows that the model was 92.6% accurate in the afternoon of day 1. Even though the ISCST3 model is not perfect, its poor performance in the afternoon of day 3, which yielded the lowest value of IOA, can be deemed acceptable because $d \geq 0.4$ [50].

Fractional bias (FB) gives an indication (sign) of bias along the receptor and provides estimates of extremities in under predictions (-) or over predictions (+). From Table 1, FB values are positive except for day 1 in the afternoon, indicating over prediction of radon concentrations. The negative FB value of -0.05 in the afternoon of day 1 indicates that the model under predicted the radon concentration. However, this value can be considered acceptable as it is below -0.5. Another notable deviation from acceptable limits is observed in the afternoon of day 3 as 0.614 value is beyond the 0.5 recommended limit of acceptable model fit. Moreover, day 3 afternoon anomalies correspond to the lowest index of agreement values discussed above. In all other cases, the model can be deemed acceptable with acceptable degree of reliability.

Except day 3 afternoon, NMSE values for all the days are found to be < 0.5, which also indicates satisfactory model performance for those modelling scenarios. Conversely, the 0.670 NMSE value for day 3 afternoon exceeded the 0.5 limit, a trend similarly observed with FB values and IOA values.

Table 1 mostly shows MG > 1 (over prediction) except for day 1 afternoon, in which MG < 1 (under prediction). The highest degree of over-prediction occurred on the afternoon of day 3, with a peak value of 1.887. This indicates a significant prevalence of over-prediction, surpassing acceptable limits. Only day 1 morning and day 2 afternoon yielded MG < 1.25 to regard the model as acceptable. Day 1 afternoon MG = 0.951 was the only one below 1, indicating under prediction. FAC2 values were found to be greater than 0.8, signifying an acceptable performance by the model. However, high FAC2 values for day 3 afternoon should be treated circumspectly.

In summary, ISCST3 model showed a constant trend with minimal variability in the IOA, NMSE and FAC2 values. The only exception is day 3 afternoon for all results and to a lesser extent day 1 afternoon for FB values. Evaluation of the model performance showed that the modelled day 3 afternoon outputs did not correspond to the measured data, an indication that the model was performing poorly.

3.3. Model validation: Source apportionment

RaA and RaB to radon ratios are listed in Table 2, which omits (from the analysis) ratio values > 1. As discussed in section 2.4 and shown in Figure 4, daughter concentrations cannot surpass parent radon concentration. Typical outdoor ratios for radon progeny concentrations are 0.8/1 for RaA/Rn and 0.78/1 for RaB/Rn [51], which may however not be applicable to the current scenario.

Table 2 : RaA and RaB to radon-222 ratios

Date and receptor point	RaA (Bq/m³)	RaB (Bq/m³)	Rn (Bq/m³)	RaA/Rn ratio	RaB/Rn ratio
Day 1 (Morning)					
9:30 (A)	17.91±1.90	6.35±0.45	10.25±0.23	1.747±0.230	0.619±0.058
11:12 (B)	3.00±1.30	0.55±0.26	8.50±0.21	0.353±0.163	0.065±0.032
12:00 (C)	2.16±0.97	0.38±0.20	8.44±0.21	0.256±0.121	0.044±0.026
Day 1 (Afternoon)					
13:32 (A)	2.15±0.84	0	6.13±0.18	0.351±0.147	0
14:30 (B)	7.11±1.66	7.17±0.51	15.50±0.28	0.459±0.115	0.463±0.047
15:26 (C)	2.23±0.88	0	6.19±0.19	0.361±0.153	0
16:12 (D)	1.68±0.85	0.50±0.20	4.63±0.16	0.363±0.195	0.108±0.047
Day 2 (Afternoon)					
13:08 (A)	1.69±0.69	0.48±0.18	10.75±0.23	0.157±0.068	0.045±0.018
13:54 (B)	0	0	20.63±0.32	0	0
14:50 (C)	3.09±0.91	0.73±0.20	10.94±0.24	0.282±0.089	0.067±0.020
15:49 (D)	8.04±1.30	0.41±0.19	7.66±0.19	1.049±0.194	0.054±0.027
Day 3 (Morning)					
7:39 (A)	17.8±2.4	4.05±0.47	20.63±0.32	0.862±0.131	0.196±0.026
8:35 (B)	11.8±2.1	3.71±0.42	20.13±0.32	0.588±0.111	0.184±0.024
9:25 (C)	12.3±1.9	1.96±0.35	23.38±0.34	0.527±0.091	0.084±0.016
10:28 (D)	6.2±1.4	0.17±0.26	10.69±0.23	0.583±0.145	0.016±0.024
11:14 (E)	6.9±1.3	1.29±0.25	20.25±0.32	0.344±0.070	0.064±0.013
Day 3 (Afternoon)					

13:00 (A)	2.03±1.02	0.25±0.21	13.13±0.26	0.155±0.080	0.019±0.016
13:52 (B)	3.08±0.88	0.36±0.18	20.50±0.32	0.150±0.045	0.017±0.009
15:24 (C)	1.52±0.71	0.49±0.19	8.38±0.21	0.182±0.089	0.059±0.024
Day 4 (Afternoon)					
13:19 (A)	6.17 ±1.23	1.53±0.26	6.19±0.18	0.997±0.227	0.247±0.049
14:12 (B)	4.84±1.27	1.00±0.26	13.38±0.26	0.361±0.102	0.075±0.020
15:04 (C)	2.66±0.92	0	10.88±0.24	0.245±0.090	0
16:04 (D)	0.52±0.69	0.52±0.20	8.38±0.21	0.062±0.084	0.062±0.026
Day 5 (Morning)					
8:02 (A)	15.3±2.3	3.35±0.42	19.88±0.32	0.770±0.125	0.168±0.025
8:50 (B)	11.4±1.9	2.03±0.32	8.31±0.21	1.367±0.259	0.245±0.047
9:43 (C)	6.7±1.5	1.05±0.26	8.13±0.20	0.822±0.202	0.128±0.041

A common feature in the results shown in Table 2 is that RaA/Rn ratios are always greater than RaB/Rn ratios. From Figure. 4, RaA reached equilibrium with radon in about 20 minutes while RaB took more than 2 hours to approach equilibrium. Therefore, considering only radon decay, more RaA will be formed in a short time compared to RaB, hence the ratio differences. In addition, the atmospheric radon concentration changes daily, and its transport depend on the vertical temperature gradient, wind speed and air turbulence.

The extreme daily ratios were 0.997:0.247 and 0.150:0.017 (RaA/Rn:RaB/Rn) on day 4 afternoon and day 3 afternoon respectively. The results in Table 2 reveal deviations from the radon decay and ingrowth of radon daughter shown in Figure 4. It is important to note that the ingrowth period can vary depending on the level of mixing in the pollution cloud. Specifically, parcels of air with "clean" air tends to lower the ratios, whereas parcels of air

containing radon daughters leads to higher ratios. Notably, such contamination can originate within the same "pollution" cloud as a result of intermixing within that cloud. This means that that the pollution cloud itself may not be well-mixed, and the contamination is not influenced only by any external sources.

This demonstrates that more complex processes are involved. For example, radon with 'age' ≅ 5 min in Figure 4 is expected to have an appropriate RaA/Rn ratio of about 0.700 and a corresponding RaB/Rn ratio of about 0.08. In contrast, the RaA/Rn ratio of 0.770 for day 5 morning in Table 2 corresponds to a high RaB/Rn ratio of 0.168. In this instance, the air from the source may be subjected to some contamination. From these ratios, a definite inference can be drawn concerning the "age" of radon daughters at each receptor point. The RaB/Rn ratio of 0.017 suggests a minimum growth period of about 3 minutes, given that RaB attains 1.7% of equilibrium in about 3 minutes. For the highest observed RaB/Rn value of about 0.247, the corresponding time of growth is about 16 minutes. Ingrowth period can increase or decrease depending on contamination level and type. That is, contamination by "clean" air will decrease the ratios whereas contamination by air containing radon daughters will increase the ratios.

Results from back-trajectory distance calculations are presented in Table 3 and depicted in Figures 6 to 11. These results excluded all ratios > 1 and receptor point B on day 2 afternoon as highlighted earlier. Two other excluded results are receptor B on day 1 (14:30 afternoon) and receptor A on day 4 (13:19 afternoon) due to extremely out of range distances stretching from four to nine kilometers.

Table 3: Source apportionment results from back calculations

Date and receptor point	RaA/ Rn	RaB/R n	Bateman times (s) (RaA/Rn)	Bateman times (s) (RaB/Rn)	Velocity (m/s)	Distance (m) (RaA)	Distance (m) (RaB)
Day 1 (Morning)							
11:12 (B)	0.353	0.065	125	350	5.3	660	1848
12:00 (C)	0.256	0.044	90	270	5.4	480	1441
Day 1 (Afternoon)							
13:32 (A)	0.351	0.000	125	0	5.1	631	0
15:26 (C)	0.361	0.000	176	0	2.7	475	0
16:12 (D)	0.363	0.108	177	490	2.4	418	1156
Day 2 (Afternoon)							
13:08 (A)	0.157	0.045	55	272	3.9	217	1072
14:50 (C)	0.282	0.067	98	350	3.2	311	1111
Day 3 (Morning)							
7:39 (A)	0.862	0.196	520	760	2.6	1352	1976
8:35 (B)	0.588	0.184	280	735	2.9	803	2108
9:25 (C)	0.527	0.084	200	420	4.2	843	177
10:28 (D)	0.583	0.016	280	80	5.2	1460	418
11:14 (E)	0.344	0.064	120	340	4.5	540	1530
Day 3 (Afternoon)							
13:00 (A)	0.155	0.019	55	165	2.7	149	446
13:52 (B)	0.150	0.017	53	160	3.3	176	530
15:24 (C)	0.182	0.059	70	330	3.8	264	1244
Day 4 (Afternoon)							
14:12 (B)	0.361	0.075	176	375	4.4	779	166
15:04 (C)	0.245	0.000	90	0	3.3	296	0
16:04 (D)	0.062	0.062	30	340	3.6	109	1229
Day 5 (Morning)							
8:02 (A)	0.770	0.168	180	700	1.8	322	1252
9:43 (C)	0.822	0.128	450	550	3.2	1449	1771

Figure 6: Radon source origins from back calculations for day 1 (a) morning and (b) afternoon

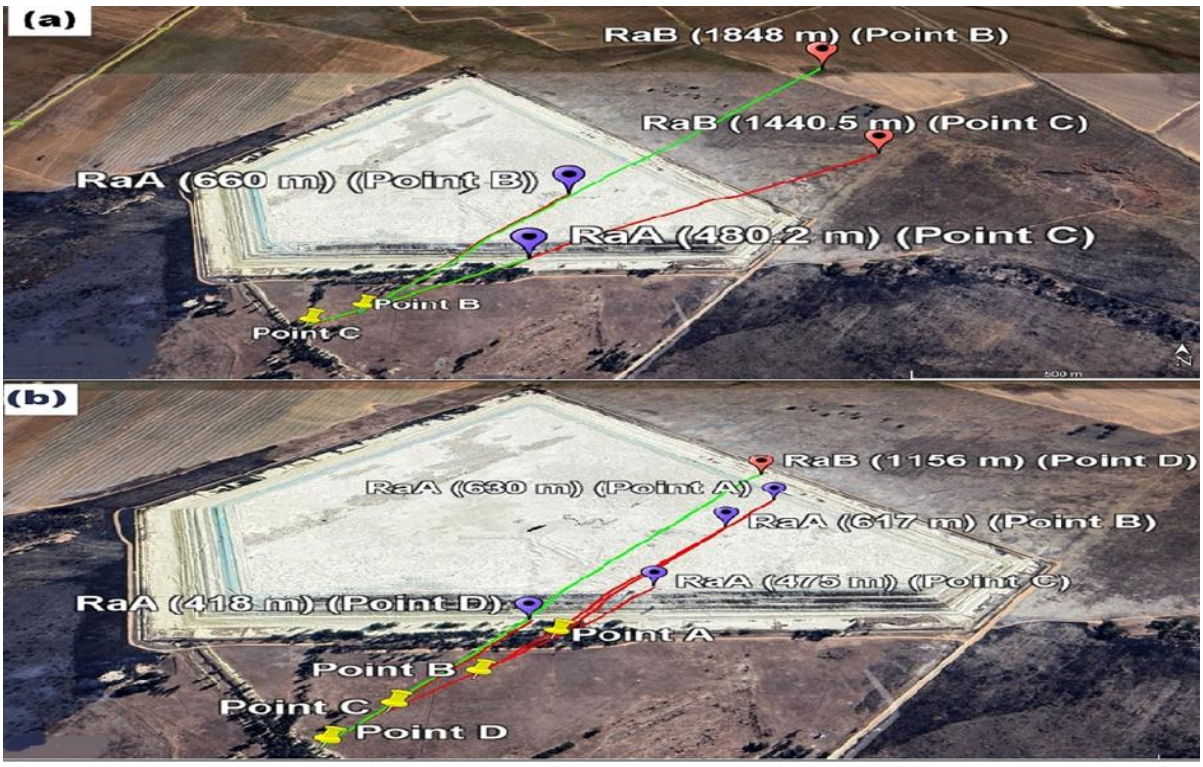

Figure 7: Radon source origins from back calculations for day 2 afternoon

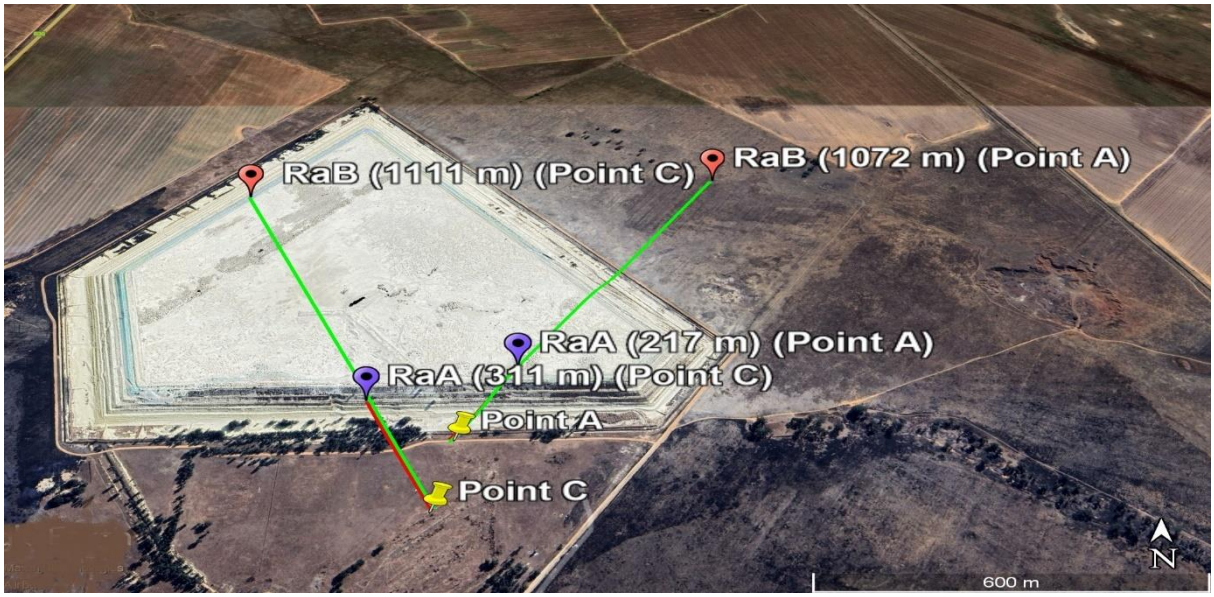

Figure 8: Day 3 morning radon source origins from back calculations for (a) receptors A, B, C and (b) receptors D and E

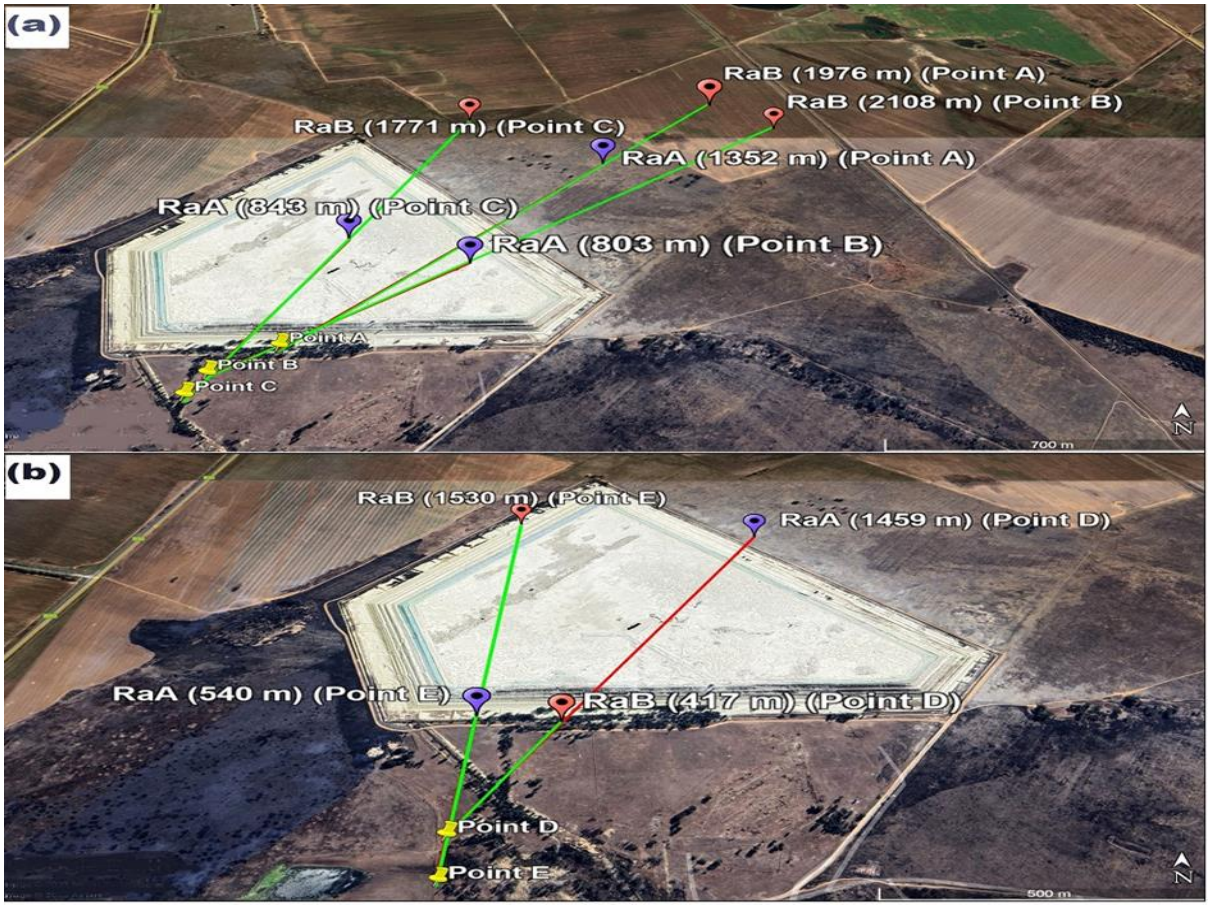

Figure 9: Day 3 afternoon radon source origins from back calculations for (a) receptor A, (b) receptors B and (c) receptor point C.

Figure 10: Day 4 afternoon radon source origins from back calculations for (a) receptors B and C and (b) receptor D.

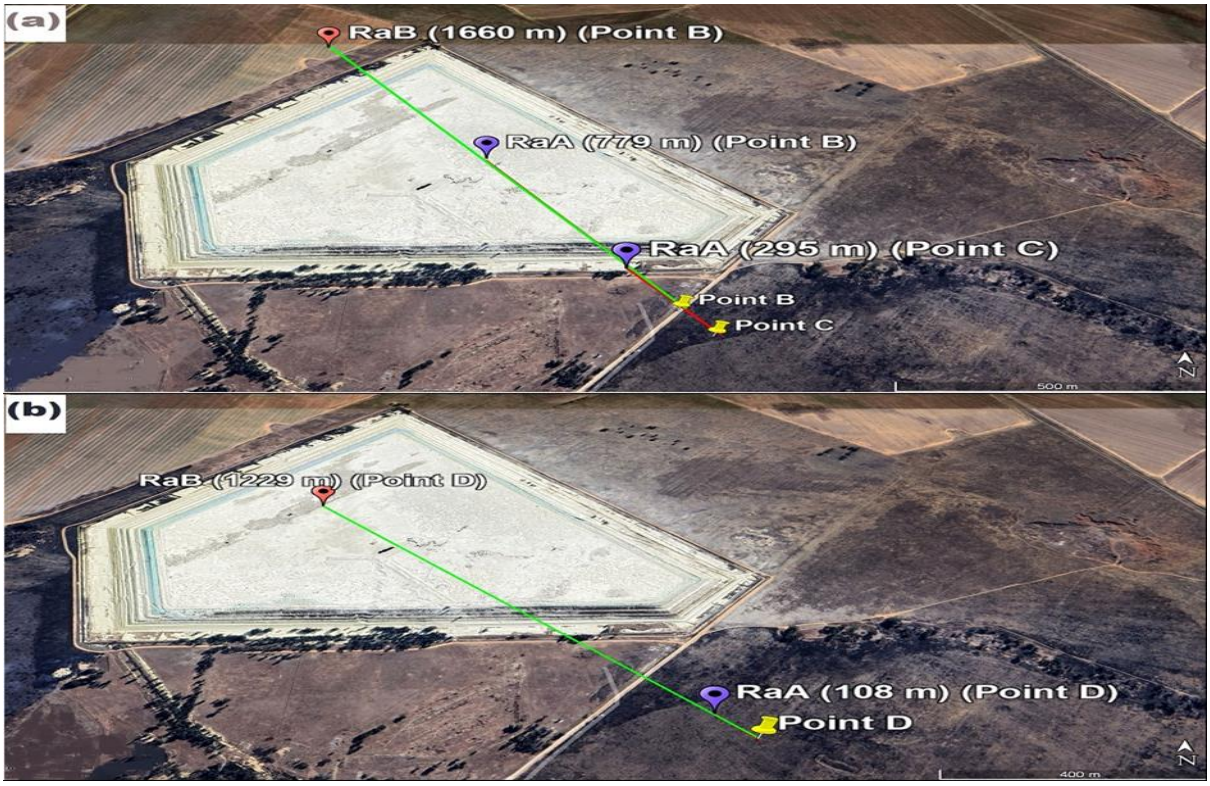

Figure 11: Radon source origins from back calculations for day 5 morning.

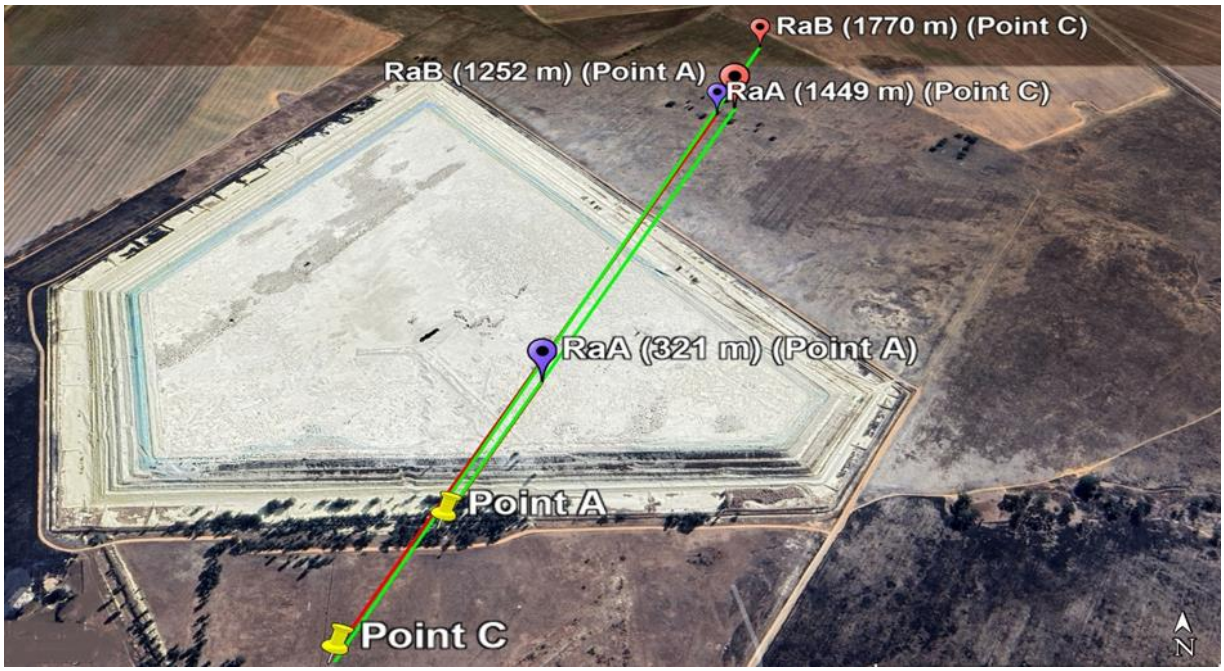

Figures 6 to 11 demonstrate that 76% of the RaA/Rn ratios shown by purple location marker, suggest that radon measurements at the receptor points originate from the tailings as predicted by the model. This supports the validity of the measurements for validation purposes. These ratios lie close to the RaA-time line in Figure 4. The other 24% of RaA/Rn ratios on day 3 morning (points A and D), day 3 afternoon (point C), day 4 afternoon (point D) and day 5 morning (point C) originate outside the perimeter up wind of the tailings dam, a deviation from the RaA-time relationship illustrated in Figure 4.

Radon concentration in the atmosphere can be approximated by RaA concentration in ambient air. Atmospheric radon concentrations reflect broader dispersion and mixing, while ambient air measurements near the ground are highly localized and sensitive to immediate environmental factors. The decay dynamics leading to RaA concentration are more pronounced and distinct in the ambient air due to localized radon exhalation and micro-meteorological influences. Therefore in-situ measurements, particularly for ambient air, provide accurate localized data reflecting real-time radon and RaA concentrations. These are critical for validating simulations. Conversely, numerical simulations provide broad insights into atmospheric radon behaviour by modeling transport, decay, and large-scale mixing. Consequently, localized in-situ data is essential for validating and refining simulation outputs, particularly for high-resolution ambient air models.

Because of its short half-life, RaA is the best indicator of how "young" or "fresh" radon is at the receptor. Furthermore, the short half-life of RaA implies that the distance travelled from the source to the receptor point will be shorter, hence most of the back trajectories reflect the radon origin located within the perimeter of the tailings dam.

In contrast to RaA/Rn ratios, 47% of RaB/Rn ratios, represented by red markers, are indicative of radon originating from within the tailings dam perimeter. As with RaA/Rn, this 47% contribution from the tailings dam is reflected in the RaB versus time graph in Figure 4.

The remaining 53% can be attributed to radon emanating from sources outside the tailings dam or poor mixing in the pollution cloud. This portion deviated from the expected RaB time curve.

The "back-calculation" or receptor model technique discussed above is highly idealised, assuming only straight-line transport from the source to the receptor. As a result, this approach is not fully applicable in the real atmosphere. Given the limited information at hand, it is not possible to trace the path of radon air packets from the source to the receptor with high accuracy. Radon movement from source to receptor may be distorted as it travels from the source such that it is divergently scattered along the direction of travel. The combined action of wind field inhomogeneities, decay properties, convective and turbulent motions may contribute to the deviation of the straight-line path described above, resulting in a curved and whirling radon path [52].

During short-range radon transport, airflow patterns may be influenced by source geometry, suchs as wake recirculation. Under these conditions, low RaA/Rn and RaB/Rn ratios indicate "fresh" radon at the receptor, which can be ascribed to the tailings dam given short travelling and time from dam to source. However, advective air mass motion can be responsible for variations in atmospheric radon concentrations [53, 54]. Because of the long half-life of 3.8 days, accumulated radon originating from different sources far away from the tailings dam may be detected at near source receptors after travelling long distances in the atmosphere. This has been particularly prominent in RaB/Rn ratio back calculations for the air mass traveling from north-east. Observations from data presented in Figures 6 to 11 suggest that most radon from RaA/Rn and RaB/Rn back calculations (coming from beyond tailings dam upwind) emanated from north-east wind direction. All off-boundary origins are relatively close to the tailings dam, and with the exception of a baseline or ambient background radon concentration present in the environment at all locations, there are no other man made radon sources in the zones where these occurred. Given the uncertainties, it can be presumed that these cases also indicate radon originating from the large tailings dam source.

The most indicative results of model validation where both RaA and RaB sources originated from the dam according to the back calculations were obtained on day 1 afternoon (point D), day 2 afternoon (point D), day 3 morning (point E) and day 3 afternoon (points A and B). These periods were characterized by low daughter radon ratios ranging between 0.15 and 0.36 for RaA/Rn ratio and between 0.017 and 0.108 for RaB/Rn ratios. Wind speeds varied between 2.4 and 4.5 m/s. The predominant wind direction was northeast for Day 1 afternoon (point D), Day 2 afternoon (point D), and Day 3 morning (point E). However, on Day 3 afternoon, the wind shifted to northwest.

Despite minimal variation in wind direction overall, the shift on Day 3 may have caused unstable conditions impacting model performance. The combination of this directional shift with low early morning wind speeds (3.72 m/s) and temperatures (10°C) likely contributed to reduced accuracy by disrupting plume dispersion and transport pathways. In addition, a micro climate with associated wind direction may have existed at the site, with different wind patterns than at the metereological station situated about 8 km to the southern direction.

These findings are consistent with the modeled results indicating with high confidence that the radon sources measured at these points were from the tailings dam. In addition, validation of radon dispersion models using other accepted gaussian models such as AERMOD can be carried out with the techniques and practices that have been introduced in this study.

4. CONCLUSIONS

While previous methods have not been properly validated [55], this study emphasised on full evaluation and validation of the model with respect to radon measurements from the tailings dam. It is accepted that the validation was done using a relatively sparse data set, due

to the difficulty of radon gas and radon daughter measurements in the chosen environment. The project's surroundings, such as accessibility, nighttime safety, remoteness, etc., made it impossible to take measurements at night. Hence, it was discouraged to leave measuring equipment unattended after dark. This complicated the comparison and result analysis, notably in relation to diurnal variations.

In this study, daytime radon concentrations were measured as a function of meteorological conditions over short time intervals of 10 minutes based on the unidirectional consideration of the wind as prescribed by the "follow the wind" method. However, during winter, when nighttime concentrations may be significantly higher, the diurnal variation of radon and radon daughter concentrations is fairly significant. Also, diurnal variations of radon exhalation variations from the tailings should be measured to account for any changes in emission rates with location and meteorology during modelling. A follow-up study in another location, preferably outside South Africa, with more long-time measurements, including night-time is suggested.

ACKNOWLEDGMENT

This research was supported by the Department of Higher Education and Training. Central University of Technology. Bloemfontein. South Africa. EDTP Seta (Northern Cape and Sol Plaatje University. Special thanks to Harmony Gold Mining Company Limited for permission to access their facility, Motheo Security (Welkom) and Sol Plaatje University Staff and Data Science Students.

FUNDING

This research was funded in part by DHET/Central University of Technology, Bloemfontein and EDTP Seta, Kimberley, Northern Cape, South Africa.

CONFLICT OF INTEREST

All authors declare that they have no conflicts of interest.

REFERENCES

[1] ZUPUNSKI, L.; STREET, R.; OSTROUMOVA, E.; et al., Environmental exposure to uranium in a population living in close proximity to gold mine tailings in South Africa, **Journal of Trace Elements in Medicine and Biology**, v. 77, p. 127-141, May 2023.

[2] ČELIKOVIĆ, I.; PANTELIĆ, G.; VUKANAC, I.; et al., Outdoor Radon as a Tool to Estimate Radon Priority Areas—A Literature Overview, **International Journal of Environmental Research and Public Health**, v. 19, n. 2, p. 662, Jan. 2022.

[3] LIEBENBERG-ENSLIN; H., VON OERTZEN; D., MWANANAWA; N., Dust and radon levels on the west coast of Namibia – What did we learn?, **Atmospheric Pollution Research**, v. 11, n. 12, pp. 2100–2109, Dec. 2020.

[4] MPHAGA, K.V.; UTEMBE, W.; SHEZI, B.; et al., Unintended Consequences of Urban Expansion and Gold Mining: Elevated Indoor Radon Levels in Gauteng Communities' Neighboring Gold Mine Tailings, **Atmosphere**, v. 15, n. 8, p. 881, Jul. 2024.

[5] UNSCEAR, "Sources and Effects of Ionizing Radiation, UNSCEAR Report to the General Assembly, with Scientific Annexes; United Nations.," UNSCEAR, New York, USA, 2008.

[6] LAKER, M.C. Environmental Impacts of Gold Mining—With Special Reference to South Africa, **Mining**, v. 3, n. 2, pp. 205–220, Mar. 2023.

[7] WINDE, F.; GEIPEL; G., ESPINA; C., et al., Human exposure to uranium in South African gold mining areas using barber-based hair sampling, **Plos One**, v. 14, n. 6, p. e0219059, Jun. 2019.

[8] RATHEBE; P.C., KHOSI, L.; KHOLOPO, M. Indoor Concentration of Radon in Residential Houses Proximal to Gold Mine Tailings – A Review of Sub-Saharan Africa Studies, **Environmental Forensics**, pp. 1–12, Nov. 2024.

[9] MOSHUPYA; P.M., MOHUBA; S.C., ABIYE; T.A., et al., In Situ Determination of Radioactivity Levels and Radiological Doses in and around the Gold Mine Tailing Dams, Gauteng Province, South Africa, **Minerals**, v. 12, n. 10, p. 1295, Oct. 2022.

[10] KOOTBODIEN, T.; IYALOO, S.; WILSON, K.; et al., Environmental Silica Dust Exposure and Pulmonary Tuberculosis in Johannesburg, South Africa, **International Journal of Environmental Research and Public Health**, v. 16, n. 10, p. 1867, May 2019

[11] MPHAGA, K.V.; UTEMBE, W.; RATHEBE, P.C.; Radon exposure risks among residents proximal to gold mine tailings in Gauteng Province, South Africa: a cross-sectional preliminary study protocol, **Frontiers in Public Health**, v. 12, p. 1328955, Mar. 2024.

[12] PAPENFUSS, F.; MAIER, A.; STERNKOPF, S.; et al., Radon progeny measurements in a ventilated filter system to study respiratory-supported exposure, **Scientific Reports**, v. 13, n. 1, p. 10792, Jul. 2023.

[13] GARZILLO, C.; PUGLIESE, M.; LOFFREDO, F.; et al., Indoor radon exposure and lung cancer risk: a meta-analysis of case-control studies, **Translational Cancer Research**, v. 6, n. S5, pp. S934–S943, Jul. 2017.

[14] BARBA-LOBO, A.; GUTIÉRREZ-ÁLVAREZ, I.; ADAME, J.A.; et al., Behavior of 222Rn, 220Rn and their progenies along a daily cycle for different meteorological situations: Implications on atmospheric aerosol residence times and Rn daughters' equilibrium factors, **Journal of Hazardous Materials**, v. 464, p. 132998, Feb. 2024.

[15] o HERNÁNDEZ-CEBALLOS, M.Á.; ALEGRÍA, N.; PEÑALVA, I.; et al., Meteorological Approach in the Identification of Local and Remote Potential Sources of Radon: An Example in Northern Iberian Peninsula, **International Journal of Environmental Research and Public Health**, v. 20, n. 2, p. 917, Jan. 2023.

[16] KUMAR, R.; JHA, V.N.; JHA, S.K.; et al., Ambient Radiological Condition around an Operating Uranium Mill Tailings Disposal Facility at Turamdih, India, **Mapan**, v. 39, n. 4, pp. 829–835, Dec. 2024.

[17] PITARI, G.; CURCI, G.; RIZI, V.; et al., Analysis of Radon Near-Surface Measurements, Using Co-Located Ozone Data, Radio-Sounding Vertical Profiles, Sensible Heat Flux and Back-Trajectory Calculation, **Pure and Applied Geophysics**, v. 181, n. 2, pp. 507–522, Feb. 2024.

[18] ŻELIŃSKI, J.; KALETA, D.; TELENGA-KOPYCZYŃSKA, J. Validation of dispersion model designated for the coke production industry, **Environmental Monitoring and Assessment**, v. 193, n. 4, p. 238, Apr. 2021.

[19] SELVARATNAM, V.; THOMSON, D.J.; WEBSTER, H.N. Validation of the Atmospheric Dispersion Model NAME against Long-Range Tracer Release Experiments, **Journal of Applied Meteorology and Climatology**, v. 62, n. 9, pp. 1165–1174, Sep. 2023.

[20] U.S. EPA, "User's Guide for the Industrial Source Complex (ISC3) Dispersion Models Volume I - User Instructions (EPA-454/B-95-003a)," **Office of Air Quality Planning and Standards, Emissions, Monitoring, and Analysis Division**: Triangle Park, NC, USA, 1995.

[21] DEMIRARSLAN, K.O.; CETIN DOĞRUPARMAK, S.; KARADEMIR, A. Evaluation of three pollutant dispersion models for the environmental assessment of a district in Kocaeli, Turkey, **Global NEST Journal**, v. 19, n. 1, pp. 37–48, Feb. 2017.

[22] GULIA, S.; NAGENDRA, S.S.; KHARE, M. Performance evaluation of ISCST3, ADMS-Urban and AERMOD for urban air quality management in a mega city of India, **International Journal of Sustainable Development and Planning**, v. 9, n. 6, pp. 778–793, 2014.

[23] SILVERMAN, K.C.; TELL, J.G.; SARGENT, E.V.; et al., Comparison of the industrial source complex and AERMOD dispersion models: case study for human health risk assessment, **Journal of the Air & Waste Management Association**, v. 57, n. 12, pp. 1439–1446, 2007.

[24] UUGWANGA, M.N.; KGABI, N.A. Dilution and dispersion of particulate matter from abandoned mine sites to nearby communities in Namibia, **Heliyon**, v. 7, n. 4, p. e06643, Apr. 2021.

[25] CHAMBERS, S.D.; CHOI, T.; PARK, S.; et al., Investigating Local and Remote Terrestrial Influence on Air Masses at Contrasting Antarctic Sites Using Radon-222 and Back Trajectories, **Journal of Geophysical Research: Atmospheres**, v. 122, n. 24, Dec. 2017.

[26] STEIN, A.F.; DRAXLER, R.R.; ROLPH, G.D.; et al., NOAA's HYSPLIT Atmospheric Transport and Dispersion Modeling System, **Bulletin of the American Meteorological Society**, v. 96, n. 12, pp. 2059–2077, Dec. 2015.

[27] STOHL, A. Computation, accuracy and applications of trajectories—A review and bibliography, **Atmospheric Environment**, v. 32, n. 6, pp. 947–966, Mar. 1998.

[28] DRAXLER, R., STUNDER, B., ROLPH, G., et al., HYSPLIT User's Guide; **Hysplit Air Resources**, 2023

[29] PÉREZ, I.A.; ARTUSO, F.; MAHMUD, M.; et al., Applications of Air Mass Trajectories, **Advances in Meteorology**, v. 2015, pp. 1–20, 2015.

[30] KGABI, N.A.; MOKGWETSI, T. Dilution and dispersion of inhalable particulate matter. In: **Ravage Of The Planet** 2009, Western Cape, South Africa, 2009, pp. 229–238.

[31] IRANKUNDA; E., TÖRÖK, Z.; MEREUȚĂ, A.; et al., The comparison between in-situ monitored data and modelled results of nitrogen dioxide (NO2): case-study, road networks of Kigali city, Rwanda, **Heliyon**, v. 8, n. 12, p. e12390, Dec. 2022.

[32] HANNUN, R.M.; ABDUL RAZZAQ, A.H. Air Pollution Resulted from Coal, Oil and Gas Firing in Thermal Power Plants and Treatment: A Review, **IOP Conference Series: Earth and Environmental Science**, v. 1002, n. 1, p. 012008, Mar. 2022.

[33] BOADH, R.; SATYANARAYANA, A.N.V.; RAMA KRISHNA, T.V.B.P. Comparison And Evaluation Of Air Pollution Dispersion Models Aermod And Iscst-3 During Pre-Monsoon Month Over Ranchi, **Journal of Industrial Pollution Control**, v. 33, n. 1, pp 674-685.

[34] IYYAPPAN, M.; BHAKIYARAJA, S; KUMARAVEL, B.; et al., Comparative Study on Multiple Point Industrial Source Complex (MPC) – Short - Term Period And Seasonal Average Period Regulatory Models, **International Journal of Engineering Research and Technology**, v. V6, n. 12, p. IJERTV6IS120007, Dec. 2017.

[35] BANDYOPADHYAY, A. Prediction of ground level concentration of sulfur dioxide using ISCST3 model in Mangalore industrial region of India, **Clean Technologies and Environmental Policy**, v. 11, n. 2, pp. 173–188, Jun. 2009.

[36] KUMAR, A.; BELLAM, N.K.; SUD, A. Performance of an industrial source complex model: Predicting long-term concentrations in an urban area, **Environmental Progress**, v. 18, n. 2, pp. 93–100, Jun. 1999.

[37] KOMATI, F.S.; NTWAEABORWA, O.M.; STRYDOM, R. Assessing environmental radon contribution by different sources near a South African gold mine tailings, **International Journal of Environmental Science and Technology**, v. 21, n. 6, pp. 5351–5366, Mar. 2024.

[38] HUANG, L.; ZHU, Y.; ZHAI, H.; et al., Recommendations on benchmarks for numerical air quality model applications in China – Part 1:, **Atmospheric Chemistry and Physics**, v. 21, n. 4, pp. 2725–2743, Feb. 2021.

[39] ZHAI, H.; HUANG, L.; EMERY, C.; et al., Recommendations on benchmarks for photochemical air quality model applications in China — NO2, SO2, CO and PM10, **Atmospheric Environment**, v. 319, p. 120-290, Feb. 2024.

[40] ROOD, A.S. Performance evaluation of AERMOD, CALPUFF, and legacy air dispersion models using the Winter Validation Tracer Study dataset, **Atmospheric Environment**, v. 89, pp. 707–720, Jun. 2014.

[41] KOMATI, F.S. Radon Dispersion From A South African Gold Mine-Tailings Dam – Measurements And Modelling, PhD, **Central University of Technology**, Bloemfontein, South Africa, 2020.

[42] BUSIGIN, A.; PHILLIPS, C.R. Uncertainties In The Measurement Of Airborne Radon Daughters, **Health Physics**, v. 39, n. 6, p. 943, Dec. 1980.

[43] IAEA, "Quality Control of Nuclear Medicine Instruments," **International Atomic Energy Agency**, Vienna, Austria, 1991.

[44] DE PAULA, V.M.; DE SÁ, L.V.; BRAZ, D.; Comparative analysis of equipment performance in nuclear medicine, **Brazilian Journal of Radiation Sciences**, v. 8, n. 1B, Sep. 2020.

[45] DEYUAN, T. Analysis of radon-222 daughters in air, **Journal of Radioanalytical and Nuclear Chemistry Letters**, v. 154, n. 1, pp. 5–21, May 1991.

[46] JCGM, "Evaluation of measurement data—Guide to the expression of uncertainty in measurement," **Int Organ Stand**, Geneva, 2008.

[47] KOMATI, F.; NTWAEABORWA, M.; STRYDOM, R. An In Toto Approach to Radon Dispersion Modelling from a South African Gold Mine Tailings, **International Journal of Environmental Research and Public Health**, v. 19, n. 13, p. 8201, Jul. 2022

[48] KOMATI, F.S.; STRYDOM, R.; NTWAEABORWA, O.M. Measurements of radon exhalation from a South African gold mine tailings using sealed tube method, **Radioprotection**, v. 56, n. 4, pp. 327–336, Oct. 2021.

[49] VENKATRAM, A.; ISAKOV, V., YUAN, J.; et al., Modeling dispersion at distances of meters from urban sources, **Atmospheric Environment**, v. 38, n. 28, pp. 4633–4641, Sep. 2004.

[50] KUMAR, A.; DIXIT, S.; VARADARAJAN, C.; et al., Evaluation of the AERMOD dispersion model as a function of atmospheric stability for an urban area, **Environmental Progress**, v. 25, n. 2, pp. 141–151, Jul. 2006.

[51] YAMASAKI, T.; IIDA, T.; SHIMO, M.; et al., Continuous Measurements of Outdoor Radon and Its Progeny Concentrations., **Japanese Journal of Health Physics**, v. 30, n. 2, pp. 149–154, 1995.

[52] STOHL, A. Trajectory statistics-A new method to establish source-receptor relationships of air pollutants and its application to the transport of particulate sulfate in Europe, **Atmospheric Environment**, v. 30, n. 4, pp. 579–587, Feb. 1996.

[53] ARNOLD, D., VARGAS, A., ORTEGA, X., Analysis of outdoor radon progeny concentration measured at the Spanish radioactive aerosol automatic monitoring network, Applied Radiation and Isotopes: Including Data, Instrumentation and Methods for Use in Agriculture, Industry and Medicine, v. 67, n. 5, pp. 833–838, May 2009.

[54] PULINETS, S.; MIRONOVA, I.; MIKLYAEV, P.; et al., Radon Variability as a Result of Interaction with the Environment, **Atmosphere**, v. 15, n. 2, p. 167, Jan. 2024.

[55] LURDES DINIS, M.; FIÚZA, A. Simulation of Liberation and Dispersion of Radon from a Waste Disposal. In: Faragó, I., Georgiev, K., and Havasi, Á. (eds), **Advances in Air Pollution Modeling for Environmental Security**, v. 54, Berlin/Heidelberg, Springer-Verlag, pp. 133–142, 2005.

LICENSE